Received 2 October 2015; revised 23 February 2016; accepted 15 March 2016. Date of publication 23 March 2016; date of current version 22 April 2016.
The review of this paper was arranged by Editor K. Shenai.

Digital Object Identifier 10.1109/JEDS.2016.2545859

On the Base Current Components in SOI Symmetric Lateral Bipolar Transistors

JENG-BANG YAU, JIN CAI, AND TAK H. NING (Fellow, IEEE)

IBM Research Division, T. J. Watson Research Center, Yorktown Heights, NY 10598, USA

CORRESPONDING AUTHOR: J.-B. YAU (e-mail: jyau@us.ibm.com)

ABSTRACT The base current components in semiconductor on insulator symmetric lateral bipolar transistors are examined in detail to yield insight into the underlying device physics. For Si-OI devices, the base current component due to recombination in the quasineutral base is negligible, the component due to injection into the emitter has a weaker than $1/N_E$ dependence because of the effect of heavy doping. The component due to recombination in the emitter–base diode space-charge region is associated with the fabrication process, and could be reduced to a negligible level with process optimization. For SiGe-OI devices, the effect of heavy doping appears to be less than for Si-OI devices. The result is higher maximum current gain for SiGe-OI devices than for comparably doped Si-OI devices.

INDEX TERMS Bipolar junction transistor, high-level injection, silicon-on-insulator, symmetric junction.

I. INTRODUCTION

The characteristics of a bipolar transistor are usually expressed in terms of the dependence of its collector and base currents as a function of the base–emitter junction voltage V'_{BE} and the collector-to-emitter voltage V'_{CE}. For an SOI (Semiconductor on Insulator) symmetric lateral bipolar transistor, these device internal voltages are related to the voltages V_B, V_E and V_C applied to the device terminals as indicated in Fig. 1. Also shown in Fig. 1 are the device structure and cross section for modeling purposes [1].

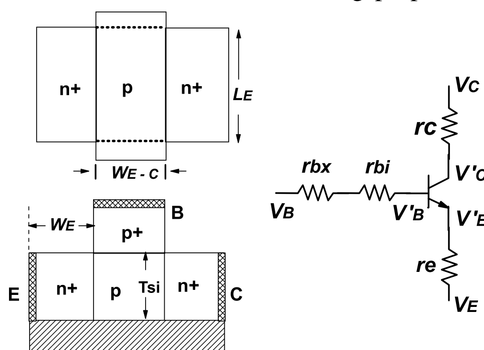

FIGURE 1. **Device structure top view (top left) and cross section (bottom left), and device junction and terminal voltages (right). (After [1]).**

Figure 2 shows the typical Gummel plots for the measured collector and base currents in a typical Si-OI NPN transistor

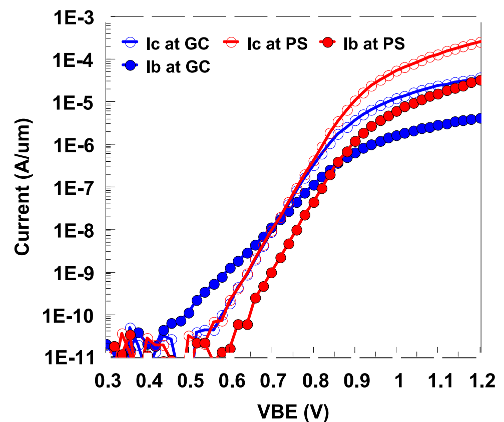

FIGURE 2. **Typical Gummel plots of the currents, measured with $V_{BC} = 0$, in a Si-OI symmetric lateral NPN device before silicide formation (GC) and after silicide formation (PS). The devices have emitter doping concentration $N_E = 4e20\ cm^{-3}$, emitter length $L_E = 1\ \mu m$ and emitter–collector spacing W_{E-C} about 180 nm.**

at two different stages of fabrication, before silicide formation (GC) and after silicide formation (PS). The currents show rapid saturation at large V_{BE} due to parasitic resistances, which are much larger before silicide formation than after silicide formation. At low V_{BE} values, the collector currents at GC and at PS are identical, and have a slope

2168-6734 © 2016 IEEE. Translations and content mining are permitted for academic research only.
Personal use is also permitted, but republication/redistribution requires IEEE permission.
See http://www.ieee.org/publications_standards/publications/rights/index.html for more information.

of approximately 60 mV/decade. However, the base currents at GC and at PS show noticeably different behavior. The implication is that we could obtain insight into the effect of fabrication process on device behavior by studying the base current components.

In this paper, we examine the physical mechanisms governing the various base current components. We then examine the base current components in Si-OI and SiGe-OI devices to gain insight into the physics of these transistors.

II. BASE CURRENT COMPONENTS

For a properly fabricated SOI lateral bipolar transistor, the three base current components are as indicated in Fig. 3. The base current density for an NPN transistor can be written as [2]

$$J_B(V'_{BE}) = \left(J_{B0,inj} + J_{B0,rec}\right) e^{qV'_{BE}/kT} + J_{B0,SC} e^{qV'_{BE}/2kT}, \quad (1)$$

where

$$J_{B0,inj} = qD_{pE} n_{ieE}^2 / N_E W_E \quad (2)$$

is the component due to hole injection into the emitter,

$$J_{B0,rec} = qW_B n_{ieB}^2 / 2\tau_{nB} N_B \quad (3)$$

is the component due to recombination in the quasineutral base region, and

$$J_{B0,SC} = qn_i W_{dBE} / \left(\tau_{n,SC} + \tau_{p,SC}\right) \quad (4)$$

is the component due to recombination in the base–emitter diode space-charge region. In these equations, D_{pE} is the diffusion coefficient for holes in the emitter, n_{ieE} is the effective intrinsic carrier density in the emitter, N_E is the emitter doping concentration, W_E is the effective emitter "junction depth" in the shallow-emitter model (see Fig. 1), W_B is the quasineutral base width, n_{ieB} is the effective intrinsic carrier density in the base, τ_{nB} is the electron lifetime in the base, N_B is the base doping concentration, W_{dBE} is the width of the base–emitter space-charge region, and $\tau_{n,SC}$ and $\tau_{p,SC}$ are the electron and hole lifetimes, respectively, in the base–emitter space-charge region.

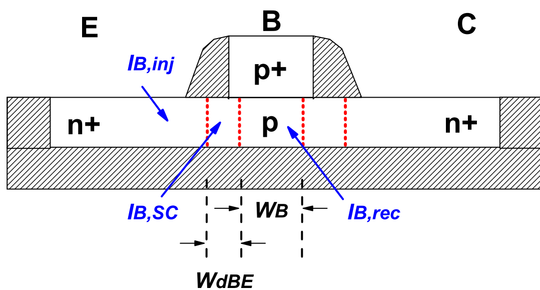

FIGURE 3. Schematic illustrating the base current components in an SOI lateral bipolar transistor. When the currents are measured at $V_{BC} = 0$, there is no base current originating from the base–collector diode space-charge region. (After [2]).

At room temperature and for bias voltages where the effect of parasitic resistances is negligible, the explicit voltage dependence in (1) suggests that the injection component and the recombination component have a 60mV/decade behavior in a Gummel plot, while the space-charge region component has a 120mV/decade behavior. This difference in behavior suggests that at low V_{BE}, e.g., less than 0.7 V, the space-charge region component may not be negligible and it may even dominate. At large V_{BE}, e.g., greater than about 0.8 V, the space-charge region component should be negligible compared to the other components. By focusing on the measured currents at large V_{BE} where the space-charge component is negligible, we should be able to determine the contribution from the injection and recombination components.

A. CURRENT GAIN AS FUNCTION OF COLLECTOR CURRENT

To that end, let us examine the measured current gain as a function of collector current. Figure 4 is a plot of the measured current gains as a function of collector current for the two devices (same physical device at two different stages of fabrication) in Fig. 2. In a symmetric lateral bipolar transistor, high-injection effect in the base causes the measured collector current to increase with base–emitter junction voltage at a rate slower than $\exp(qV'_{BE}/kT)$. The physical mechanisms will be discussed in the sub-section below. For a base doping concentration of 2e18 cm^{-3}, high-injection effect is negligible for $V'_{BE} < 0.9$ V [3]. As long as high-injection is negligible, the measured collector current is proportional to $\exp(qV'_{BE}/kT)$ and can be used to indicate the base–emitter junction voltage. From Fig. 2, we can infer that a collector current of 10^{-8} A/μm corresponds to a base–emitter junction voltage of 0.7 V. Therefore, a collector current of 2.3×10^{-5} A/μm would correspond to a base–emitter junction voltage of 0.9 V. These junction voltages are indicated in Fig. 4.

The GC device, with its large 120mV/decade base current component, shows current gain increasing with collector current at low currents. Without silicide, the large parasitic resistances limit the maximum base–emitter junction voltage attainable in the GC device to slightly larger than 0.9 V for an applied V_{BE} of 2 V, which is not large enough to cause appreciable high-injection effect. As a result, the maximum measured collector current was only about 0.1 mA/μm, with the current gain starting to saturate but still rising.

With silicide, the parasitic resistances of the PS device are much smaller. As a result, the PS device was able to reach a maximum base–emitter junction voltage significantly larger than 0.9 V and a maximum collector current of more than 10^{-3} A/μm, for the same applied V_{BE} of 2 V. With a much smaller 120mV/decade base component, the PS device shows nearly flat current gain at low currents and appreciable current gain roll off at very large currents where high-injection effect is significant. It should be noted that the measured maximum current gains of the two devices were about the same. This should not be a surprise since the two devices

were actually the same physical device at two different stages of fabrication.

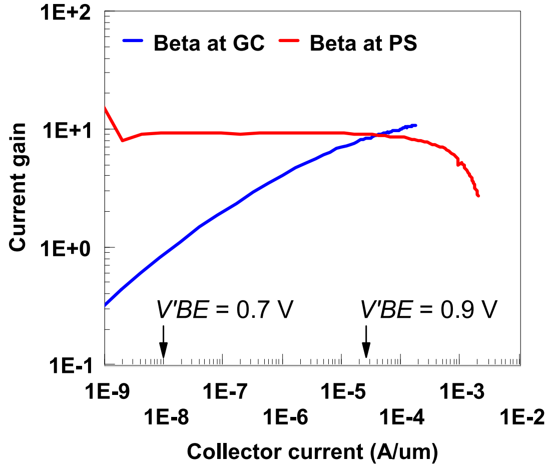

FIGURE 4. Measured current gains plotted as a function of collector current for the same two devices in Fig. 2. The base–emitter junction voltages of 0.7 V and 0.9 V during measurement are indicated.

B. PEAK CURRENT GAIN AND CURRENT GAIN ROLL OFF

The equation for I_C that is valid for arbitrary base–emitter junction voltage is [3]

$$I_C = A_E J_{C0}(V'_{BE}) \exp(qV'_{BE}/kT), \tag{5}$$

With $J_{C0}(V'_{BE})$

$$= \frac{qD_{nB}n_{ieB}^2}{N_B W_B}\left[1 + \frac{1}{4}\left(\sqrt{1 + \frac{4n_{iB}^2 \exp(qV'_{BE}/kT)}{N_B^2}} - 1\right)\right]^{-1}. \tag{6}$$

At large V'_{BE}, I_C varies explicitly as $\exp(qV'_{BE}/2kT)$. Even at small V'_{BE}, say $V'_{BE} < 0.8$ V, the measured I_C varies as $\exp(qV'_{BE}/kT)$ only if the quasineutral base width W_B remains constant. For devices with W_B comparable to or smaller than the base–emitter and base–collector diode space-charge layer widths W_{dBE} and W_{dBC}, W_B is modulated appreciably by a combination of V_{BE} and by the mobile carriers in the space-charge region [1], [3]. The net result is that the Gummel plot of the collector current of a narrow-base device at room temperature often shows a slope slightly larger than 60 mV/decade even for $V_{BE} < 0.8$ V. For devices with relatively wide base regions, the measured collector current should show a 60mV/decade behavior until high-injection effect starts to set in, causing the collector current characteristics to transition from 60mV/decade towards 120mV/decade.

For devices with heavily doped ($> 10^{20}$ cm^{-3}) emitter regions, there should be negligible high-injection effect in the measured base current [3]. As a result, the base current is expected to show 120mV/decade behavior only at small V'_{BE} (e.g., in Fig. 2). At large V'_{BE}, the measured base current should increase with V'_{BE} as $\exp(qV'_{BE}/kT)$.

The net result is that when the current gain, which is the ratio I_C/I_B, is plotted as a function of collector current, it should rise initially, due to the 120mV/decade base current component, reach a plateau and then roll off at vary large collector currents. This explains the observed current gains shown in Fig. 4.

C. DETERMINING THE BASE CURRENT COMPONENTS

Since the relatively flat current gain, in the case of the PS device, or the maximum current gain, in the case of the GC device, occur where the 120mV/decade base current component is negligible, the measured peak current gain is determined primarily by the 60mV/decade base current components. That is, we should be able to analyze the measured base current by writing

$$I_B = I_{B,inj} + I_{B,rec} + I_{B,SC}, \tag{7}$$

with the 60mV/decade component given by

$$I_{B,inj} + I_{B,rec} \approx I_C/\beta_{peak}, \tag{8}$$

where β_{peak} is the measured peak current gain. Once the 60mV/decade component is thus determined, the 120mV/decade component $I_{B,SC}$ can be determined from (7).

It should be noted that when the measured current gain shows definite roll off at very high currents, e.g., the PS device in Fig. 4, the peak value of the current gain is unambiguous. When the current gain does not reach a plateau or roll off, e.g., the GC device in Fig. 4, simply using the maximum measured current gain in (8) results in an over-estimation of the 60mV/decade base current component, which in turn results in an under-estimation of the 120mV/decade base current component.

It should also be noted that the explicit $\exp(qV'_{BE}/2kT)$ dependence for the space-charge region recombination base current was derived with certain assumptions and approximations [4]. These include the assumptions that only mid-gap states contribute to recombination and the carrier lifetimes are independent of doping concentration. In addition, $I_{B0,SC}$, given by (4), has a weak dependence on V_{BE} through the dependence of W_{dBE} on V_{BE}. For a given N_B, W_{dBE} is larger for a lightly doped emitter than for a heavily doped emitter. The net is that the Gummel plot of the base current component due to recombination in the base–emitter diode space-charge may not show exactly 120mV/decade behavior.

III. ANALYSIS APPLIED TO SI-OI DEVICES

Among the three base current components, only the $J_{B0,rec}$ term depends on N_B explicitly. The $J_{B0,SC}$ term depends on N_B indirectly through the base–emitter diode space-charge layer width W_{dBE}. For a given base region design, i.e., given combination of W_B and N_B, $J_{B0,rec}$ is inversely proportional to t_{nB}. For modeling purposes, the electron lifetime for Si devices is given by [5]

$$\frac{1}{\tau_{nB}} = 3.45\text{x}10^{-12} N_B + 0.95\text{x}10^{-31} N_B^2. \tag{9}$$

The n_{ieB} value as a function of N_B can be determined from the unified bandgap narrowing model [6]. Figure 5 is the calculated $I_{B,rec}$ at $V_{BE} = 0.7$ V for $W_B = 100$ nm as a function of N_B. The T_{si} value (SOI thickness) of 60 nm is the same as for the devices shown in Fig. 2.

Consider the N_B of 5e19 cm^{-3} point (the last data point) in Fig. 5. For a device with such a large N_B value, it should have W_B less than 10 nm [1]. That is, Fig. 5 suggests that a properly designed device with N_B of 5e19 cm^{-3} is expected to have a recombination base current < 1 pA/μm when biased at 0.7 V as indicated in Fig. 5. Comparison with the measured base current in Fig. 2 suggests that the base current component due to recombination in the quasineutral base is negligibly small even for the most heavily doped intrinsic base.

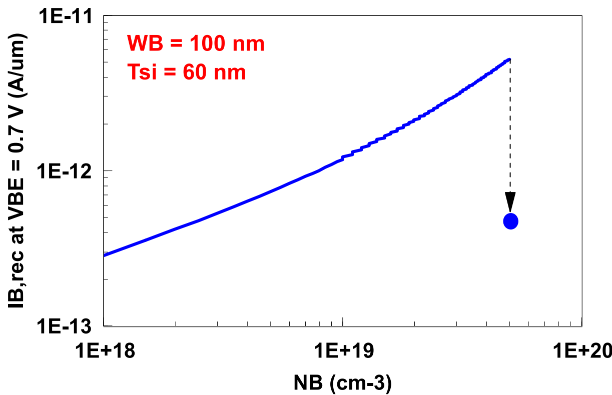

FIGURE 5. Calculated $I_{B,rec}$ for a Si-OI deviceat $V_{BE} = 0.7$ V as a function of N_B. The solid circle indicates $I_{B,rec}$ for the device design with $N_B = 5e19$ cm^{-3}.

A. THE INJECTION-INTO-EMITTER COMPONENT

With recombination base current being negligible, the measured 60mV/decade base current in a Si-OI transistor should be due entirely to minority carrier injection into the emitter. That is, the ratio I_C/β_{peak} gives the injection base current $I_{B,inj}$. Figure 6 is a plot of the measured I_C/β_{peak} for three devices with the same N_E but different N_B. It shows no definitive dependence on N_B, as expected from the fact that $J_{B0,inj}$ is independent of N_B.

Figure 7 is a plot of the measured I_C/β_{peak} for two devices with the same N_B but different N_E. It shows that the injection base current component for the device with N_E of 4e20 cm^{-3} is smaller than that for the device with N_E of 1e20 cm^{-3}. The dependence of $J_{B0,inj}$ on N_E can be inferred from (2). The diffusion coefficient D_{pE} is relatively independent on N_E for N_E larger than 2e19 cm^{-3}. Since the two devices in Fig. 7 have the same physical structure, the dependence of W_E on N_E, if any, is expected to be weak. That means, to first order, $J_{B0,inj}$ is proportional to n_{ieE}^2/N_E. Since bandgap narrowing due to heavy doping increases with N_E, n_{ieE} increases with N_E, offsetting the effect of N_E on base current. This explains why the injection base current of the device with

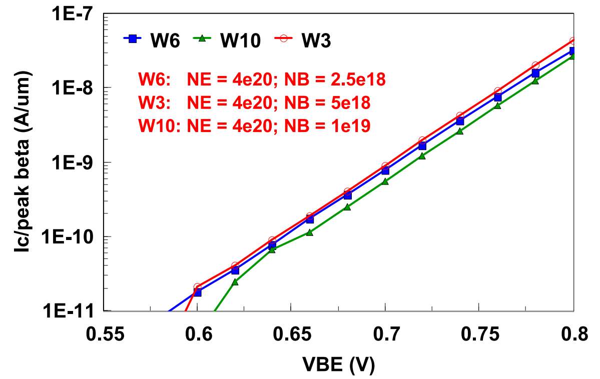

FIGURE 6. Typical plot of the ratio I_C/β_{peak} for Si-OI devices with the same heavily doped emitter but different base doping concentrations.

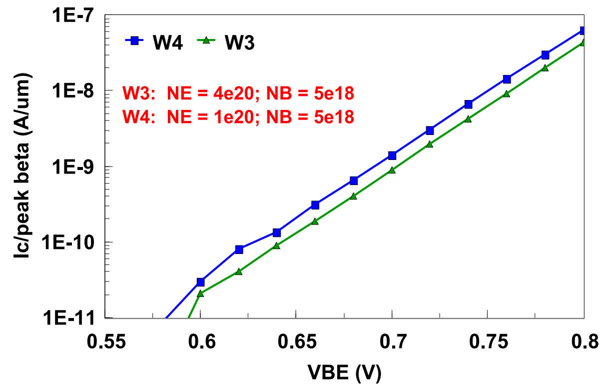

FIGURE 7. Typical plot of the ratio I_C/β_{peak} for Si-OI devices with different emitter doping concentrations.

N_E of 4e20 cm^{-3} is smaller than that of the device with N_E of 1e20 cm^{-3} by a factor less than 4.

B. THE SPACE-CHARGE-REGION RECOMBINATION COMPONENT

Once the 60mV/decade base current component has been determined, the 120mV/decade component is simply the difference between the measured base current and the 60mV/decade component. Figure 8 plots the base current components analyzed in this manner for the transistors shown in Fig. 2. The I_C/β_{peak} plots at GC and at PS are practically the same, as expected, while the 120mV/decade component at GC is about 100x that at PS. Apparently the silicide formation steps (which involve RTA at 400° C in nitrogen) result in about 100x reduction of the defects responsible for recombination in the base–emitter diode space-charge region. Figure 8 suggests that the base current, when analyzed in this manner, could be a tool for studying defects associated with fabrication process steps.

IV. ANALYSIS APPLIED TO SIGE-OI DEVICES

Recently, SiGe-OI symmetric lateral NPN transistors were reported and the base currents were analyzed in the same manner [2]. Here we examine the results in greater depth to gain further insight into the physics of SiGe-OI transistors.

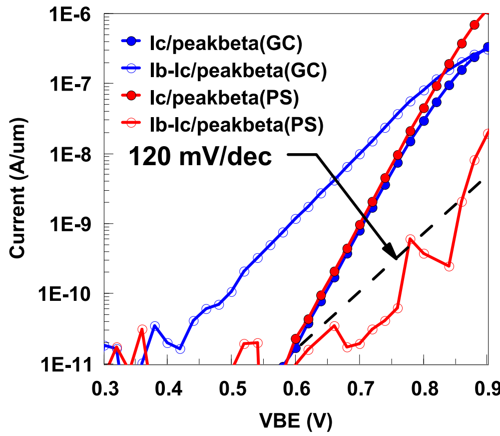

FIGURE 8. The 60mV/decade and 120mV/decade components of the base currents for the two transistors in Fig. 2.

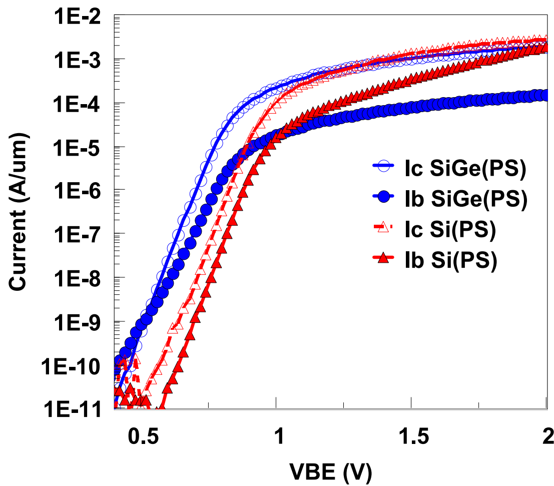

FIGURE 9. Comparison of currents, measured at $V_{BC} = 0$, of a SiGe-OI lateral NPN with a Si-OI lateral NPN. Both devices were processed through the silicide formation step (PS). The devices have an emitter length $L_E = 0.2$ µm. Compared to the Si device, the collector current (the part with 60mV/decade slope) of the SiGe device is shifted to the left by about 130 mV. (After [2]).

As a reference, the Gummel plots for the SiGe and Si devices reported in are shown here in Fig. 9. The SiGe-OI devices were fabricated using epitaxially grown SiGe on 10-nm Si-OI substrate [2]. That is, both SiGe and Si devices in Fig. 9 have Si/BOX interface. These devices were processed through the silicide step (PS) in fabrication. The measured current gain as a function of collector current is shown in Fig. 10. Also indicated in Fig. 10 are the measured collector currents at base–emitter junction voltage of 0.7 V inferred from Fig. 9. The maximum applied V_{BE} during current measurement was 2 V for both transistors. Figure 10 suggests that, at applied V_{BE} of 2 V, the Si device was able to attain a much larger collector current than the SiGe device, suggesting the SiGe device having larger parasitic resistances than the Si device. This is consistent with Fig. 9 showing flatter curves at large V_{BE} for the SiGe device than for the Si device.

In Fig. 10, the Si device shows current gain roll off similar to the PS device in Fig. 2, as expected. The SiGe device was not able to attain the large base–emitter junction voltage needed to show appreciable current gain rolling off. It only gives a hint of start of roll off. [However, after the metallization step (M1), the parasitic resistance of the SiGe device was much reduced. We will return to discuss this SiGe device at M1 later in Section IV-B.]

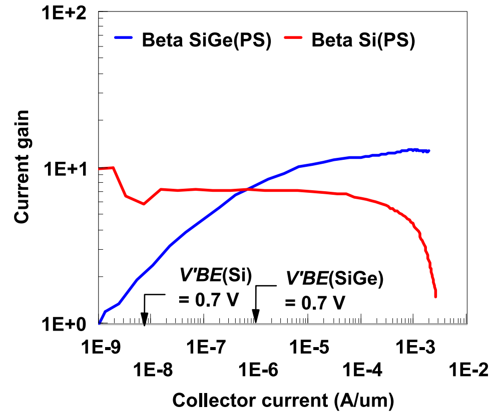

FIGURE 10. Measured current gains as a function of collector current for the same two devices in Fig. 9. The collector currents at which the devices have a base–emitter junction voltage of 0.7 V are indicated.

A. INSIGHT FROM THE BASE CURRENT COMPONENTS

The measured current gain for the Si device appears noisy for collector currents less than 10^{-8} A/µm. For purposes of analyzing the base current for insight into device physics, we chose the peak current gain at a current greater than 10^{-8} A/µm. Figure 11 is a plot of the 60mV/decade and 120 mV/decade base currents thus obtained for the Si and SiGe devices of Fig. 9. As expected, the Si device in Fig. 11 has about the same 60mV/decade and 120mV/decade base currents as the Si device at PS in Fig. 8. The base current components of the SiGe device, on the other hand, suggest something quite interesting.

First, the 120mV/decade base current component for the SiGe device is larger than that for the Si device by a factor of almost 100x. With the emitter much more heavily doped than the base ($N_E = 4e20$ cm^{-3} and $N_B = 2.5e18$ cm^{-3}), the emitter–base diode is a one-sided junction with space-charge region primarily on the base side. From (4), we see that the space-charge region recombination base current component is proportional to $n_i/(t_{n,SC} + t_{p,SC})$. The collector currents in Fig. 9 suggests that the base region energy gap of the SiGe device is about 130 meV smaller than that of the Si device, suggesting n_i for the SiGe device to be about 12x that for the Si device, accounting for 12x of the 100x larger space-charge region recombination current. The remaining factor of about 8x is probably due to residual implantation damage of As into the emitter/collector regions [2].

Comparing the 60mV/decade components for the two devices in Fig. 11 shows that the component for the SiGe

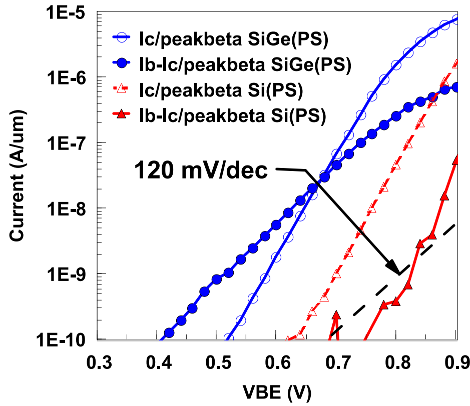

FIGURE 11. The 60mV/decade and 120mV/decade components of the base currents of the SiGe-OI and Si-OI NPN devices in Fig. 9. Compared to the Si device, the 60mV/decade base current component of the SiGe device is shifted to the left by about 110 mV.

device is shifted to the left by about 110 mV. This shift is smaller than the 130 mV shift for the collector current shown in Fig. 9. The difference in shift is about 20 meV. A possible explanation is as follows. It has been reported that effective bandgap narrowing due to heavy doping is smaller for SiGe than for Si [7]. For the Si device, the calculated difference in effective bandgap narrowing, using the unified apparent bandgap narrowing model [6], between the emitter ($N_E = 4e20$ cm^{-3}) and the base ($N_B = 2.5e18$ cm^{-3}) is about 70 meV. The reported bandgap narrowing for p-type doped SiGe, between N_a of 1-7e18 cm^{-3} and N_a of 1-2.5e20 cm^{-3} is only about 40 meV [7]. If we assume the difference in effective bandgap narrowing between the n-type SiGe emitter ($N_E = 4e20$ cm^{-3}) and the p-type SiGe base ($N_B = 2.5e18$ cm^{-3}) is also about 40 meV, it would suggest the shift of the injection base current components for the SiGe device from that of the Si device should be about 30 mV smaller than the shift of the collector currents for the SiGe device from that of the Si device. That is, the observed smaller shift in injection base current component compared to the observed shift in collector current is likely due to the smaller doping-induced bandgap narrowing effect in SiGe compared to Si.

B. COMPARING SIGE DEVICE AT PS AND AT M1

The SiGe device discussed in the previous section was processed through the silicide formation step (PS). The same device was subsequently processed through a copper metallization step (M1). Figure 12 compares the Gummel characteristics of the same device at PS and at M1. The background leakage current (about 10^{-9} A/μm) of the M1 device suggests the metallization process steps needed optimization. Ignoring the background leakage current, Fig. 12 shows that the 60mV/decade collector currents at PS and at M1 are the same, as expected. Figure 13 shows the measured current gains as a function of collector current. It shows that, for the same maximum applied V_{BE} of 2 V, the M1 device was able to reach a larger maximum collector current than the PS device, suggesting smaller series resistances for the M1 device. This is consistent with the characteristics at large V_{BE} in Fig. 12.

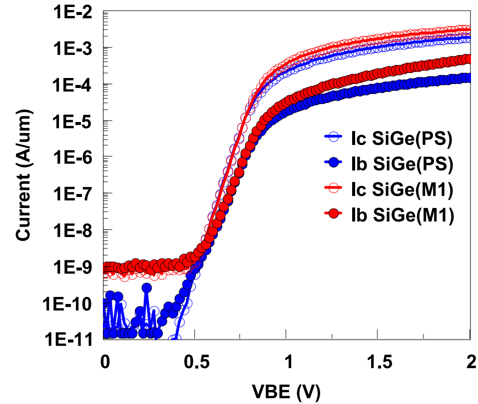

FIGURE 12. Gummel plots measured at $V_{BC} = 0$ for the SiGe-OI lateral NPN shown in Fig. 9 at two stages of fabrication process, after silicide (PS) and after copper metallization (M1).

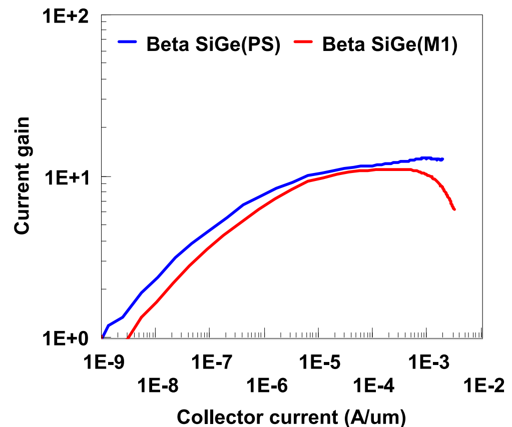

FIGURE 13. Measured current gains as a function of collector current for the devices in Fig. 12.

Figure 13 shows noticeable difference in the measured current gains. The M1 device clearly shows current gain roll off at large collector currents while the PS device shows a just a hint of current gain starting to roll off at the maximum measured current. Also, the measured peak current gain is slightly larger for the PS device (12.8 versus 11.1). Yet the 60mV/decade base current components at PS and at M1, shown in Fig. 14, appear indistinguishable. This should not be surprising because the 60mV/decade base current component is determined by the injection of holes into the emitter region, i.e., Eq. (2), which should not be affected by the metallization process.

C. INSIGHT FROM LIGHTLY DOPED EMITTER

Next let us consider a SiGe-OI NPN having the same base doping concentration, $N_B = 2.5e18$ cm^{-3}, but a much lower emitter doping concentration, $N_E = 5e19$ cm^{-3}. This

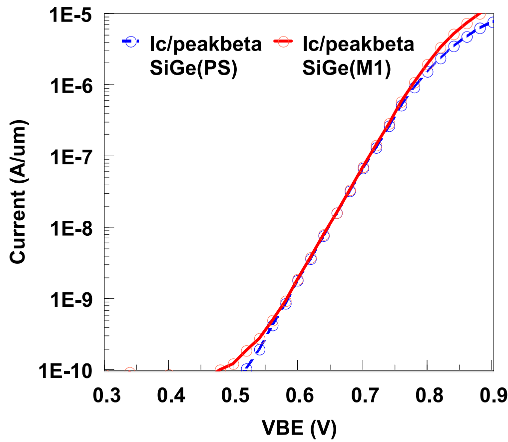

FIGURE 14. The 60mV/decade components of the base currents of the SiGe-OI at PS and at M1. The slightly larger current at $V_{BE} < 0.55$ V for the M1 device is due to the background current at M1. The slightly larger current at $V_{BE} > 0.8$ V is due to the smaller parasitic resistance of the M1 device.

$N_E = 5\text{e}19$ cm^{-3} device was fabricated on the same wafer as the $N_E = 4\text{e}20$ cm^{-3} device discussed above. The measured collector and base currents are shown in Fig. 15. The currents for the SiGe device with N_E of 4e20 cm^{-3} from Fig. 9 are also included for comparison. It shows that I_C (the 60mV/decade part) for the $N_E = 4\text{e}20$ cm^{-3} device is larger than that for the $N_E = 5\text{e}19$ cm^{-3} device. This is consistent with the fact that a larger emitter/collector implantation dose leads to smaller final emitter-to-collector separation, and hence smaller quasineutral base width and larger collector current.

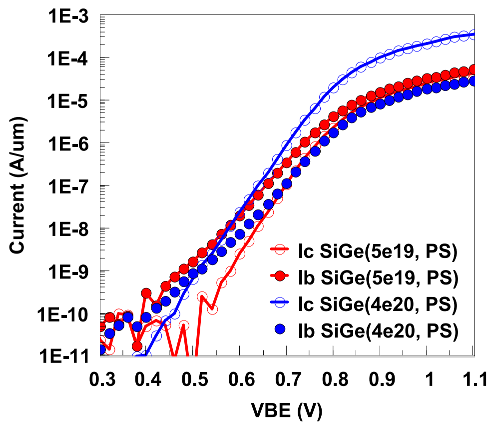

FIGURE 15. Comparison of the currents, measured at $V_{BC} = 0$, of two SiGe-OI devices with different emitter doping concentrations from the same wafer processed through the silicide formation step. The devices have an emitter length $L_E = 0.2$ μm and mask dimension for emitter/collector implantation of approximately 180 nm. (After [2]).

The explanation for the larger observed current gain roll off in the $N_E = 5\text{e}19$ cm^{-3} device as shown in Fig. 16 is as follows. As discussed earlier in Section II-B, the quasineutral base width W_B is modulated by V_{BE} and V_{BC}, and by the mobile carriers in the base–emitter and base–collector space-charge regions, causing the collector current to increase with V'_{BE} more slowly than $\exp(qV'_{BE}/kT)$. With more lightly doped emitter/collector regions, the base–emitter diode and the base–collector diode of the $N_E = 5\text{e}19$ cm^{-3} device have space-charge regions that extend into the emitter side and the collector side, respectively. (In the case of $N_E = 4\text{e}20$ cm^{-3} device, the space-charge regions are confined to the base side only, with little extension on the emitter or collector sides.) This leads the $N_E = 5\text{e}19$ cm-3 device to have larger base–emitter and base–collector space-charge regions and hence larger base-width modulation effect by mobile carriers in the space-charge regions. Therefore, any collector current roll off effect, hence current gain roll off effect, is larger in the $N_E = 5\text{e}19$ cm^{-3} device than in the $N_E = 4\text{e}20$ cm^{-3} device.

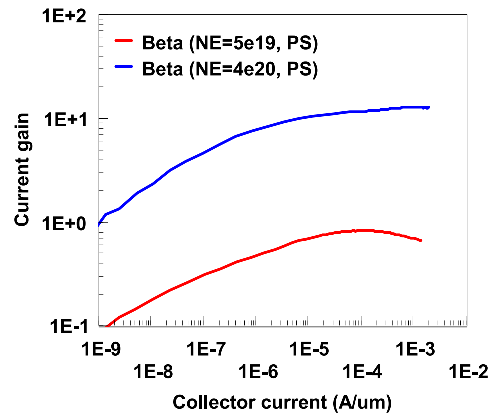

FIGURE 16. Measured current gain as a function of collector current for the same two devices in Fig. 15.

The 60mV/decade and 120mV/decade base current components for the $N_E = 5\text{e}19$ cm^{-3} device are shown in Fig. 17. Also plotted for comparison are the corresponding components for the $N_E = 4\text{e}20$ cm^{-3} device. At $V_{BE} = 0.6$ V, the 60mV/decade base current component for the $N_E = 5\text{e}19$ cm^{-3} device is larger than that for the $N_E = 4\text{e}20$ cm^{-3} device by a factor or only 1.6, instead of 8 (the N_E ratio of the two devices). The small ratio could be due to heavy doping effect (see Fig. 7 and the discussion thereof).

Figure 17 indicates a somewhat larger 120mV/decade base current for the $N_E = 5\text{e}19$ cm^{-3} device than for the $N_E = 4\text{e}20$ cm^{-3} device. For the $N_E = 4\text{e}20$ cm^{-3} device, the emitter doping concentration is much larger than the base doping concentration ($N_B = 2.5\text{e}18$ cm^{-3}), leading to a one-sided emitter–base junction with the space-charge region confined primarily to the base side. Only the emitter implantation damage at the very edge of the emitter region contributes to space-charge region recombination. For the $N_E = 5\text{e}19$ cm^{-3} device, the emitter–base diode has a two-sided junction with the space-charge region extending appreciably into the emitter region. More emitter implantation damage ends up in the space-charge region, leading to larger space-charge region recombination current.

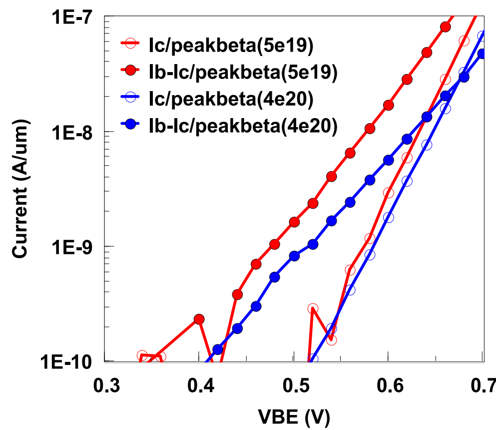

FIGURE 17. The 60mV/decade (circles) and 120mV/decade (solid dots) base current components for the two SiGe-OI devices in Fig. 15.

V. CONCLUSION

A methodology has been developed for analyzing the measured base current in SOI symmetric lateral bipolar transistors. A detailed study of the base current components offers deep insight into physical mechanisms, especially fabrication-related physics, governing the operation and characteristics of the transistors. For Si-OI devices, the base current component due to recombination in the quasineutral base is negligible. The component due to recombination in the emitter–base diode space-charge region is a function of device fabrication process, and could be reduced to a negligible level with process optimization. In addition, if the heavy doping effect were absent in Si-OI devices, the current gain would be larger than observed by a factor of about 15. [As described in Fig. 11, the difference in bandgap narrowing due to heavy doping between emitter and base is about 70 mV, which corresponds to a factor of 15 of difference in the base and collector currents.] For SiGe-OI devices, the effect of heavy doping appears to be less than for Si-OI devices. The implication is that for a Si-OI device and a SiGe-OI device having identical physical dimensions and doping profiles, the SiGe-OI device has a higher maximum current gain than the Si-OI device.

The base current component $I_{B,SC}$ is due to the recombination in the base–emitter diode space-charge region. It includes the contribution from recombination due to interface traps at the semiconductor/BOX interface within the space-charge-region boundary. There is no contribution from interface traps within the quasineutral base region (W_B). For probing recombination due to interface traps within the quasineutral base region, the SOI lateral bipolar transistor should be operated in a MOSFET mode and the so-call DCIV (direct-current current-voltage) method be employed for base (substrate) current analysis [8]–[10]. In that case, the thickness of the SOI layer should be thin in order to suppress the base current component $I_{B,inj}$ due to injection from the base into the emitter.

REFERENCES

[1] T. H. Ning and J. Cai, "On the performance and scaling of symmetric lateral bipolar transistors on SOI," *IEEE J. Electron Devices Soc.*, vol. 1, no. 1, pp. 21–27, Jan. 2013.

[2] J.-B. Yau *et al.*, "SiGe-on-insulator symmetric lateral bipolar transistors," in *Proc. IEEE S3S Conf.*, Rohnert Park, CA, USA, 2015, pp. 1–2.

[3] J. Cai *et al.*, "On the device design and drive-current capability of SOI lateral bipolar transistors," *IEEE J. Electron Devices Soc.*, vol. 2, no. 5, pp. 105–113, Sep. 2014.

[4] C. T. Sah, R. N. Noyce, and W. Shockley, "Carrier generation and recombination in p-n junction and p-n junction characteristics," *Proc. IRE*, vol. 45, no. 9, pp. 1228–1243, Sep. 1957.

[5] S. E. Swirhun, Y.-H. Kwark, and R. M. Swanson, "Measurement of electron lifetime, electron mobility and band-gap narrowing in heavily doped p-type silicon," in *IEEE IEDM Tech. Dig.*, Los Angeles, CA, USA, 1986, pp. 24–27.

[6] D. B. M. Klaassen, J. W. Slotboom, and H. C. de Graaff, "Unified apparent bandgap narrowing in n- and p-type silicon," *Solid-State Electron.*, vol. 35, no. 2, pp. 125–129, 1992.

[7] Ž. Matutinović-Krstelj, V. Venkataraman, E. J. Prinz, J. C. Sturm, and C. W. Magee, "Base resistance and effective bandgap reduction in n-p-n Si/Si$_{1-x}$Ge$_x$/Si HBT's with heavy base doping," *IEEE Trans. Electron Devices*, vol. 43, no. 3, pp. 457–466, Mar. 1996.

[8] A. Neugroschel *et al.*, "Direct-current measurements of oxide and interface traps on oxidized silicon," *IEEE Trans. Electron Devices*, vol. 42, no. 9, pp. 1657–1662, Sep. 1995.

[9] C.-T. Sah, A. Neugroschel, K. M. Han, and J. T. Kavalieros, "Profiling interface traps in MOS transistors by the DC current-voltage method," *IEEE Electron Device Lett.*, vol. 17, no. 2, pp. 72–74, Feb. 1996.

[10] J. Cai and C.-T. Sah, "Monitoring interface traps by DCIV method," *IEEE Electron Device Lett.*, vol. 20, no. 1, pp. 60–63, Jan. 1999.

JENG-BANG YAU received the Ph.D. degree in electrical engineering from Princeton University, in 2002. He joined IBM T. J. Watson Research Center, in 2006, and has been involved in innovative FDSOI CMOS technologies. He is currently actively engaged in various advanced research works, including the SOI lateral bipolar transistors. His achievements include demonstration of tunable power/performance modulation in thin-body FDSOI enabled by dual-back bias and FDSOI radiation dosimeters.

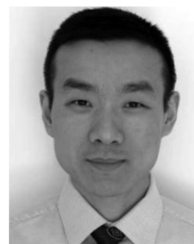

JIN CAI received the B.S. degree in physics from Fudan University, China, and the M.S. and Ph.D. degrees in electrical engineering from the University of Florida. From 2000 to 2015, he was with IBM T. J. Watson Research Center, Yorktown Heights, NY. In 2015, he joined TSMC, Hsinchu, Taiwan. He was a recipient of two IBM Outstanding Technical Achievement Awards for his contributions to advanced CMOS technology development.

TAK H. NING (M'75–SM'81–F'87) received the Ph.D. degree from the University of Illinois at Urbana–Champaign, in 1971. He joined IBM Research, Yorktown Heights, NY, USA, in 1973, where he is an IBM Fellow. He has been recognized with several awards, including the Electrochemical Society 2007 Gordon E. Moore Medal, the 1991 IEEE Jack A. Morton Award, and the 1989 IEEE Electron Devices Society J. J. Ebers Award. He is a member of the National Academy of Engineering, and a fellow of the American Physical Society.